Raman and photoluminescence spectroscopy of SiGe layer evolution on Si(100) induced by dewetting

A. A Shklyaev, V. A. Volodin, Mathieu Stoffel, Hervé Rinnert, M. Vergnat

▶ **To cite this version:**

A. A Shklyaev, V. A. Volodin, Mathieu Stoffel, Hervé Rinnert, M. Vergnat. Raman and photoluminescence spectroscopy of SiGe layer evolution on Si(100) induced by dewetting. Journal of Applied Physics, In press, 123 (1), pp.015304. 10.1063/1.5009720 . hal-02168861

HAL Id: hal-02168861
https://hal.science/hal-02168861

Submitted on 29 Jun 2019

HAL is a multi-disciplinary open access archive for the deposit and dissemination of scientific research documents, whether they are published or not. The documents may come from teaching and research institutions in France or abroad, or from public or private research centers.

L'archive ouverte pluridisciplinaire **HAL**, est destinée au dépôt et à la diffusion de documents scientifiques de niveau recherche, publiés ou non, émanant des établissements d'enseignement et de recherche français ou étrangers, des laboratoires publics ou privés.

Raman and photoluminescence spectroscopy of SiGe layer evolution on Si(100) induced by dewetting

A. A. Shklyaev,[1,2] V. A. Volodin,[1,2] M. Stoffel,[3] H. Rinnert,[3] and M. Vergnat[3]
[1]*A.V. Rzhanov Institute of Semiconductor Physics, SB RAS, Novosibirsk 630090, Russia*
[2]*Novosibirsk State University, Novosibirsk 630090, Russia*
[3]*Université de Lorraine, Institut Jean Lamour UMR CNRS 7198, B.P. 70239, 54506 Vandœuvre-lès-Nancy Cedex, France*

(Received 19 October 2017; accepted 21 December 2017; published online 4 January 2018)

High temperature annealing of thick (40–100 nm) Ge layers deposited on Si(100) at ~400 °C leads to the formation of continuous films prior to their transformation into porous-like films due to dewetting. The evolution of Si-Ge composition, lattice strain, and surface morphology caused by dewetting is analyzed using scanning electron microscopy, Raman, and photoluminescence (PL) spectroscopies. The Raman data reveal that the transformation from the continuous to porous film proceeds through strong Si-Ge interdiffusion, reducing the Ge content from 60% to about 20%, and changing the stress from compressive to tensile. We expect that Ge atoms migrate into the Si substrate occupying interstitial sites and providing thereby the compensation of the lattice mismatch. Annealing generates only one type of radiative recombination centers in SiGe resulting in a PL peak located at about 0.7 and 0.8 eV for continuous and porous film areas, respectively. Since annealing leads to the propagation of threading dislocations through the SiGe/Si interface, we can tentatively associate the observed PL peak to the well-known dislocation-related D1 band. *Published by AIP Publishing.* https://doi.org/10.1063/1.5009720

I. INTRODUCTION

Solid-state dewetting is a process that can drastically modify the properties of surface layers. It is widely used for the formation of various metal layer surface morphologies.[1–3] The dewetting of SiGe layers was observed recently on both Si(111)[4] and Si(100)[5,6] substrates. A detailed investigation of the dewetting process would be thus highly desirable both from the scientific and applied viewpoints. SiGe heterostructures are usually grown far from equilibrium, thereby producing strained structures due to the Si-Ge lattice mismatch. The main processes that release the strain under post-growth annealing are Si-Ge interdiffusion and dislocation nucleation.[7,8] In the case of dewetting, strain energy minimization additionally occurs through the formation of Si substrate areas that are not covered with SiGe films, thus reducing the size of interface areas between the deposited film and the substrate.[9]

The dewetting in a Si-Ge system can induce the formation of submicron- and micron-sized SiGe particles on Si substrates,[6] which can serve as dielectric particles with a refractive index $n > 3$. The light scattering on such particles leads to the generation of electrical and magnetic resonances, according to Mie theory, when the relation $d \sim \lambda/n$ between the particle size (d) and the wavelength of light (λ) is satisfied.[10,11] This leads to an essential redistribution of the electromagnetic field around the particles. In addition, the particles can work as lenses for far-field light focusing.[12] Due to their properties, the introduction of Si or Ge Mie-resonance particle arrays can improve the performance of photodetectors, light sources, solar cells, and sensors.[13] The other result of dewetting is the formation of surface morphologies more complicated than particles, such as nets of ridges, which can substantially enhance the light absorption. Although the dewetting in the Si-Ge system leads to a spontaneous change in the surface morphology, being caused only by the total energy minimization, it can, nevertheless, be controlled. This can occur through the introduction of nucleation centers to form a new surface morphology using patterned substrates.[14] The dewetting control can ensure the quasi-random photonic nanostructure formation, for example, similar to those obtained in multistep technological processes using wrinkle lithography.[15]

The dewetting of a Ge layer deposited on Si substrates occurs at temperatures above 750 °C. It can be realized in two approaches. In one of them, Ge is deposited on Si surfaces straight at the high temperatures. It leads to the formation of different surface morphologies depending on the surface crystallographic orientation. The appearance of structures such as the net of ridges was observed on Si(111),[4] whereas compact individual islands were formed on Si(100).[16] In the other approach, about 30–100 nm thick Ge layers, initially deposited on Si(100) or Si(111) surfaces at relatively low temperatures (~400 °C), were subsequently annealed at higher temperatures. On Si(111), it leads to the formation of ridge-like structures, and it occurs suddenly on the whole surface.[4] On Si(100), a continuous film formation is observed at the initial stage of high temperature annealing, and then, it slowly transforms into a porous film. The transformation occurs through a slow movement of the boundary between the continuous and porous film areas.[5] As a result, both continuous and porous film areas can exist simultaneously on a same sample. In this work, we study the changes in the film properties along a line crossing the boundary between continuous and porous regions, using both Raman and photoluminescence

(PL) spectroscopies. We further discuss the reason for the compressive stress appearance in the Si substrate and the origin of the photoluminescence band formation in Si/Ge heterostructures after high-temperature annealing.

II. EXPERIMENTAL DETAILS

The growth experiments were carried out in an ultrahigh-vacuum chamber with a base pressure of about 1×10^{-10} Torr. A $10 \times 2 \times 0.3\,mm^3$ sample was cut from an *n*-type Si(100) wafer with a miscut angle of $<10'$ and a resistivity of 5–20 Ω cm. Clean Si surfaces were prepared by flash direct-current heating at 1250–1270 °C. A Knudsen cell with a BN crucible was used for the Ge deposition at a rate up to 1.0 nm/min. The Ge growth on Si(100) surfaces was carried out at 400 °C. The post-growth sample annealing was performed *in situ* at 850 °C. The sample temperature was measured using an IMPAC IGA 12 pyrometer. After the removal of samples from the growth chamber, their morphology was analyzed by scanning electron microscopy (SEM) using a Pioneer microscope manufactured by Raith. The chemical composition of the surface layers was measured using the energy-dispersive X-ray spectroscopy (EDX) of SEM SU8220 made by Hitachi. To obtain a better spatial resolution in EDX measurements of chemical compositions along a certain line along a sample cleavage, the incident e-beam energy was reduced to 4 keV. The use of samples with sharp Si/Ge interfaces showed that this gives 95% changes in the chemical composition within the 50 nm length across the interface.

The Raman spectra were measured at room temperature in the backscattering geometry using a T64000 Horiba Jobin Yvon spectrometer with the excitation by an Ar^+ laser with the wavelength of 514.5 nm.[17] The PL was excited by a laser diode emitting at 488 nm and detected by a multichannel InGaAs based detector, which can detect light up to 2100 nm (i.e., 0.6 eV). The laser beam, focused on the sample surface, was about 1.3 mm in diameter, and its power varied between 0.5 and 50 mW. A cryostat with a temperature stability ±0.5 K was used for the low-temperature PL study. PL measurements were performed for sample temperatures in the range from 10 to 150 K. A detailed description of the experimental setup is given elsewhere.[18]

III. SURFACE MORPHOLOGY AND Si-Ge COMPOSITION

The surface morphology of the Ge layers grown on Si(100) at 400 °C strongly depends on the deposited Ge amount. For Ge thicknesses larger than 30 nm, the morphology is composed of continuous ridges that are formed as a result of the coalescence of large dome-like islands.[5] After 60 nm Ge deposition, the surface morphology still exhibits uncovered Si(100) areas. Such surface morphologies are thermally unstable due to the lattice strain between the areas with deposited Ge and the underlying Si(100) substrate. Annealing of 60 nm thick Ge films at temperatures as high as 850 °C leads to the formation of two areas with different surface morphologies, the sizes of which depend on the annealing time and the temperature. During the first few minutes, the annealing causes a reduction of the surface roughness leading to an almost continuous film, as shown in Fig. 1(a). A further annealing initiates the transformation of the continuous film into a porous-like film [Fig. 1(b)]. The transformation occurs slowly starting preferentially at surface defects and sample edges. As a result, two different surface morphologies (flat and porous) can coexist on the sample surface.[5] Moreover, the cross-sectional SEM images [see the insets of Figs. 1(a) and 1(b)] show that the interface between the Ge film and the Si substrate remains sharp for both surface morphologies. In the inset to Fig. 1(b), one can recognize that the pores are extending into the Si substrate, well below the interface between the Ge film and the Si(001) substrate.

We then perform the cross-sectional measurements of the Si-Ge composition using EDX. The composition profiles were measured along a line crossing the interface between the substrate and the grown films. The obtained results are presented in Figs. 2(a) and 2(b) for the continuous film and in Figs. 2(c) and 2(d) for the porous film. For the continuous film [Figs. 2(a) and 2(b)], the Si-Ge composition does not vary abruptly across the interface. Instead, the interface is strongly interdiffused having a width of about 10–30 nm. Our measurements further show that the continuous film is alloyed with an average Si content of about 50%. After the continuous film transformation into the porous one [Figs. 2(c) and 2(d)], the compositional changes are less pronounced across the

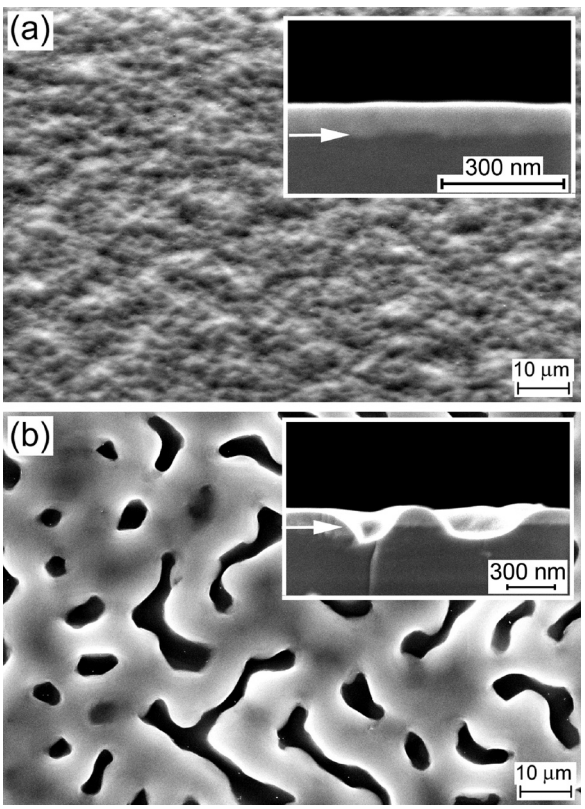

FIG. 1. SEM images of the sample surfaces after 60 nm Ge deposition on Si(100) at 400 °C followed by a subsequent annealing at 850 °C for 60 min. The top view (and cross-sectional view in the insets) of the continuous SiGe film area (a) and of the porous SiGe film area (b). The white arrows in the insets show the position of the interface.

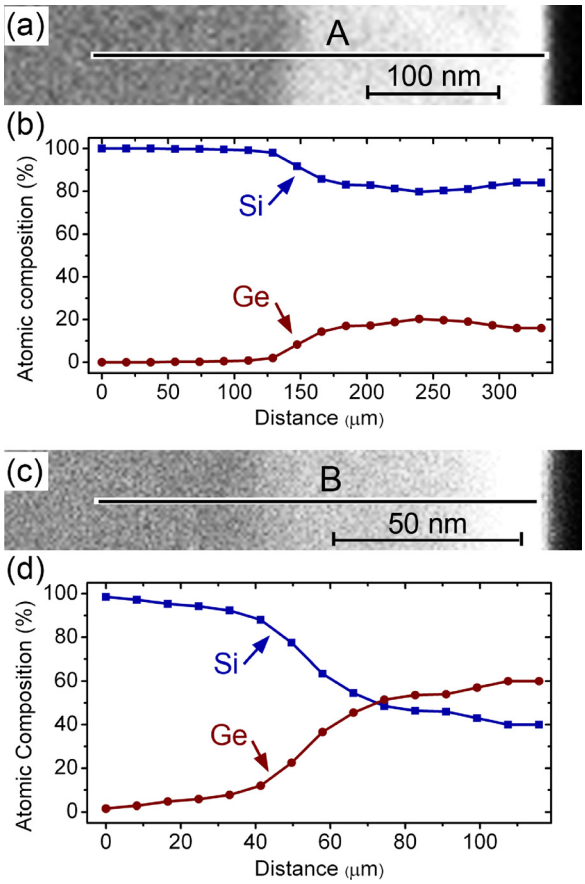

FIG. 2. EDX data for the continuous and porous films of the same sample shown in Fig. 1. The atomic composition was obtained along the lines A and B shown on the SEM images (a) and (c) for the continuous (b) and porous (d) films, respectively.

interface, the Ge content reaches only 20%. It should be noted that the latter value was measured for an area located far from the boundary between the continuous and porous films, contrary to that used for the Raman spectroscopy measurement described below.

IV. RAMAN SPECTROSCOPY CHARACTERIZATION

The Raman spectra of a 60 nm thick Ge film deposited onto Si(001) at 400 °C prior to (spectrum 1) and after the annealing at 850 °C for 1 h are shown in Fig. 3. Spectrum 2 was measured on a continuous film area, while spectrum 3 was measured on a porous film area. Spectrum 1 is characterized by two main peaks at 301.6 and 520.6 cm^{-1}, which can be associated with the Raman peaks of bulk crystalline Ge and Si, respectively (Fig. 3). The growth temperature of 400 °C is too low to initiate the Si-Ge intermixing, i.e., the possible Raman peak shifts can be produced by the strain due to the Si-Ge lattice mismatch rather than by the Si-Ge intermixing. The weak peak at 390 cm^{-1}, which is associated with the Si-Ge vibration mode, probably, originates from the Si/Ge interface.[19,20] However, the Si-Si-related vibration band being observed at 520.5–520.6 cm^{-1} indicates that the Si in the open areas of the Si substrate, which are located between the ridges of the deposited Ge films, is unstrained, since this band position is typical of unstrained Si. As for the

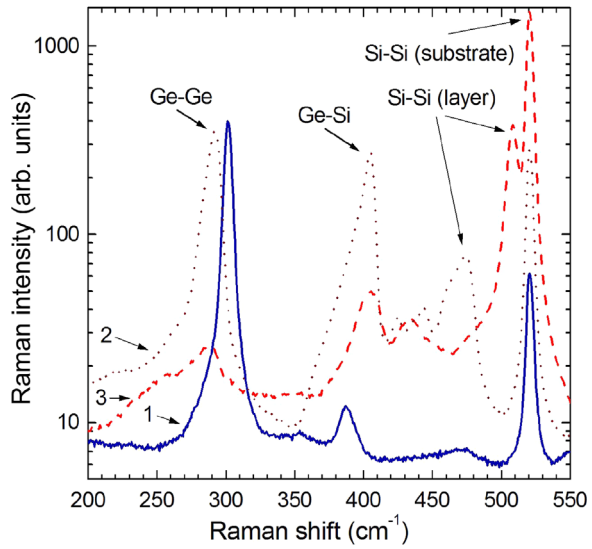

FIG. 3. Raman spectra for the 60 nm thick Ge film deposited on a Si(100) substrate at 400 °C (spectrum 1), and the similar prepared sample after the annealing at 850 °C for 30 min. Spectra 2 and 3 are measured from continuous and porous SiGe film areas, respectively.

peak from the Ge-Ge vibration band, its intensity and spectral position are predominantly determined by the top part of the deposited Ge layer, since the penetration depth is about 19 nm for the laser beam with the 514.5 nm wavelength. The Ge-Ge vibration band is observed at 301.6 cm^{-1}, which is close to its known position for unstrained Ge (~301.3 cm^{-1}).[21,22]

Significant changes in the Raman spectra were observed after the sample annealing at 850 °C. In particular, the intensity of the Ge-Si vibration mode located between 350 cm^{-1} and 450 cm^{-1} strongly increases for both the continuous and the porous film areas (spectra 2 and 3 in Fig. 3). This indicates that a strong Si-Ge intermixing takes place during the annealing and, thus, it confirms the EDX results shown in Fig. 2(b). To highlight the changes in the continuous film during its transformation into the porous film, a set of the Raman spectra were measured at 11 points along a line crossing the boundary between the continuous and the porous film areas [Fig. 4(a)]. The Ge-Ge and Ge-Si mode intensity significantly decreased, while the Si-Si mode intensity increased as a function of the distance across the boundary [Fig. 4(b)]. This behavior is expected, since the pores are protruding into the Si substrate [Fig. 1(b)], leading to Si areas which are not covered with SiGe layers. It should be noted that, despite the very short penetration depth of the laser beam for Ge, it is about 760 nm for Si. The continuous SiGe film obtained after annealing at 850 °C has a Ge content of ~0.55 [Fig. 2(b)]. This clarifies the possibility of the Si substrate-related peak observation in the Raman spectra for the continuous layers.

The dependencies presented in Fig. 4 show that the main changes in the surface layer composition occur within a width of about 100 μm. After the formation of the porous film area, slower changes continue to occur under annealing. In particular, the decrease in the intensity of the Si-Si mode, related to the substrate, is observed [Fig. 4(b)]. This indicates that the annealing causes a slow reduction of the pore sizes and that the surface morphology gradually becomes smooth. Smoothing is accompanied by the Si-Ge intermixing as

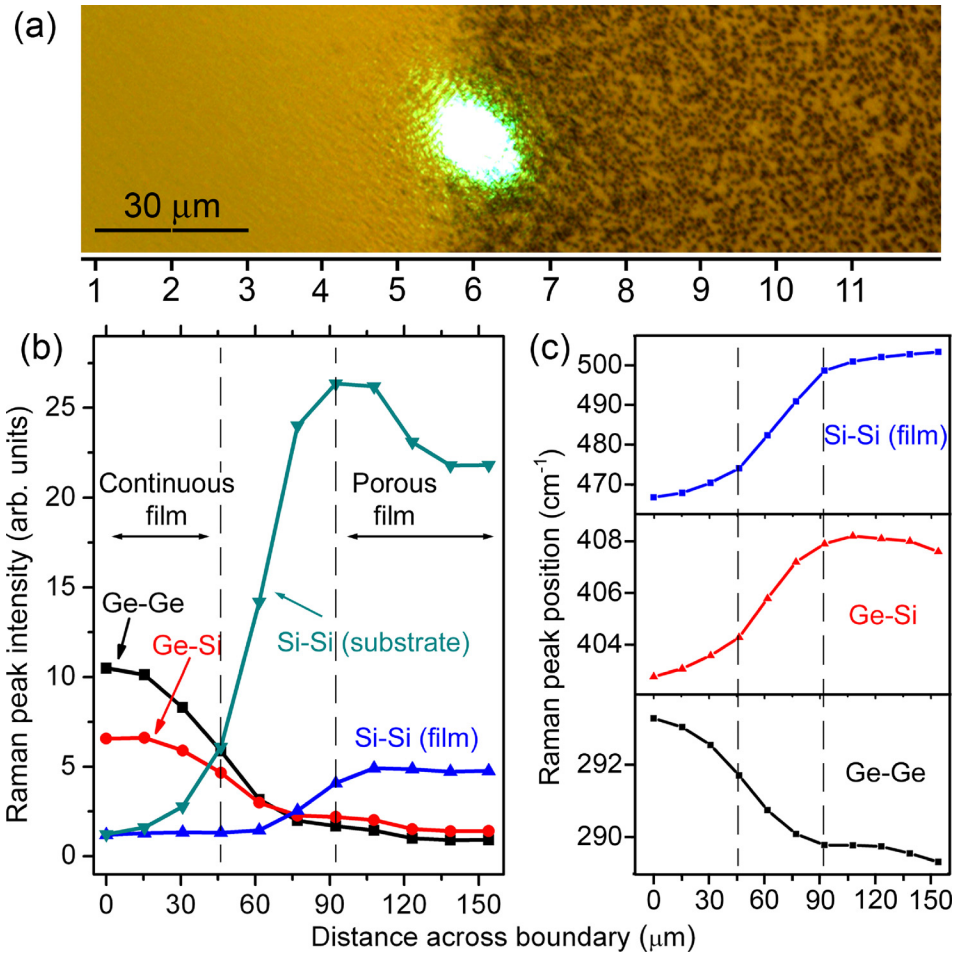

FIG. 4. Raman spectroscopy data obtained at 11 points along the line crossing the boundary between the continuous film [left side of the photograph (a)] and the porous SiGe film (on the right side). The sample was prepared by the annealing at 850 °C for 30 min of the 60 nm thick Ge film deposited at 400 °C on a Si(100) substrate. (a) The photograph of the boundary on the surface with the probing laser beam in the center corresponds to point 6. (b) The intensity of the Raman peaks marked in the spectra shown in Fig. 3, and (c) the Raman shifts of Ge-Ge, Si-Ge, and Si-Si (of the film) vibration bands as a function of the distance across the boundary. The continuous and porous film areas are indicated in (b).

shown by the evolution of the Ge-Ge Raman peak position [Fig. 4(c)].

The Raman data allow us to obtain the Si-Ge composition and strain evolution caused by the continuous film transformation into the porous one. We will use linear approximations between the Raman peak shifts from one side and Ge content x and strain ε from the other side. Our analysis showed that reasonable results can be obtained using the following parameters in the linear approximation:[21,23]

$$\omega_{SS} = 520.6 - 70x - 830\varepsilon, \tag{1a}$$

$$\omega_{SG} = 400.5 + 12x - 575\varepsilon, \tag{1b}$$

$$\omega_{GG} = 282.2 + 19.4x - 385\varepsilon, \tag{1c}$$

where ω_{SS}, ω_{SG}, and ω_{GG} are the Raman peak positions of the Si-Si, Si-Ge, and Ge-Ge vibration modes. The parameters in Eq. (1) are similar to those derived in Refs. 19, 21, and 23–25 with the corrected positions of the Si-Si and Ge-Ge peaks of bulk Si and Ge measured using our equipment. Equations (1a) and (1c) provide good approximations for a wide range of x values, whereas the linear approximation for ω_{SG} is generally used for $0 < x < 0.5$. From Eqs. (1a) and (1b), and from Eqs. (1b) and (1c), the following expressions for x can be derived:

$$x_{SSSG} = \frac{1.44 \times (\omega_{SG} - 400.5) - (\omega_{SS} - 520.6)}{87.3}, \tag{2a}$$

$$x_{SGGG} = \frac{1.49 \times (\omega_{GG} - 282.2) - (\omega_{SG} - 400.5)}{16.9}, \tag{2b}$$

respectively. The values of x, calculated from the experimental data using Eqs. (2a) and (2b), as a function of the distance across the boundary between the continuous and porous films are shown in Fig. 5(a). Assuming that the EDX spectroscopy data are correct, Eq. (2a) better describes the x values for $x > 0.5$. In the range $x < 0.5$, both Eqs. (2a) and (2b) give similar results. The obtained x value for the porous film area decreases during the porous film formation and its annealing. It eventually reaches 0.2 after a longer annealing, which is consistent with the Ge content determined in the porous area far from the boundary using EDX spectroscopy.

The ε values can be obtained using the calculated x values and Eq. (1a) written in the form

$$\varepsilon = \frac{520.6 - \omega_{SS} - 70x_{SSSG}}{830}. \tag{3}$$

According to Eq. (3), the obtained strain is positive (corresponding to a compressive stress) in the continuous film area. However, the strain becomes negative (corresponding to a tensile stress) in the porous film area [Fig. 5(b)]. The Ge films grown on Si substrates at temperatures close to 500 °C normally undergo the compressive stress due to the lattice mismatch between Si and Ge. Our results show that the continuous film remains compressive even after the annealing at

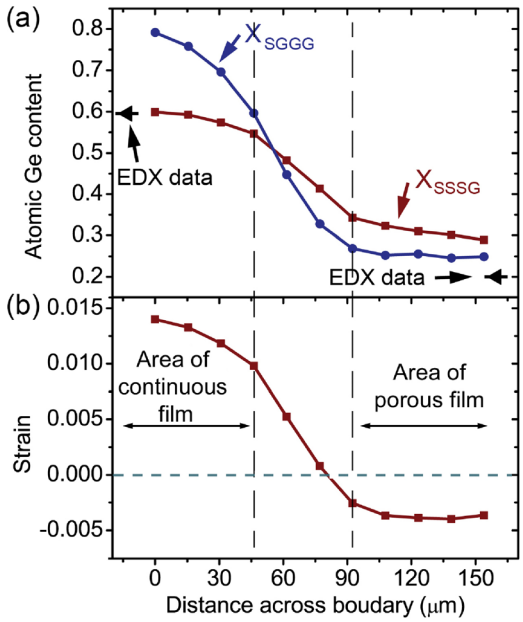

FIG. 5. Ge content x and strain ε obtained from the Raman data presented in Fig. 4(c) as a function of the distance across the boundary between the continuous and porous films. The dotted lines separate the area of the data obtained for the continuous film, the intermediate area and the porous film.

850 °C. At such high temperatures, both Si-Ge intermixing and dislocation nucleation at the interface reduce the strain to a minimum value. The following film cooling to room temperature can lead to the appearance of a tensile strain, since Ge has a bigger thermal expansion coefficient than Si.[26,27] This can happen when the effect of thermal expansion is greater than the remaining compressive stress caused by the lattice mismatch. This can occur in the case of the porous film formation leading to the appearance of the tensile stress. A similar effect was observed by Zhao *et al.* after annealing at 680 °C for 10 min of an initially weakly strained Ge film on Si.[27]

The Si-Si vibration band related to the substrate downshifts by about $\Delta\omega \sim 0.2\,\mathrm{cm}^{-1}$ when the probing area moves along the continuous film to the boundary with the porous film (Fig. 6). This shift may be caused by the lattice strain. Using the relation

$$\varepsilon_S = \frac{-(\omega_{SS} - 520.6)}{830} \tag{4}$$

derived from Eq. (1a) with $x = 0$, we obtain a compressive stress in the Si substrate below the continuous film. This is quite unusual, since the continuous film is also compressive. The Si-Si Raman peak position is up-shifted when the measurement is performed in the porous film area. This leads to the appearance of a tensile stress in the upper part of the Si substrate.[28,29] In the case of the porous film, the main contribution in the Raman peak originates from the bare Si areas located in the pores, since the probing laser beam penetration depth is limited. This means that the Si-Si peak, related to the substrate, characterizes the status of Si located only in pores. The Si in pores can be tensely strained when lying under a compressive SiGe film. Indeed, calculations have shown that if Si, lying under a Ge island, is tensely strained, then Si, lying

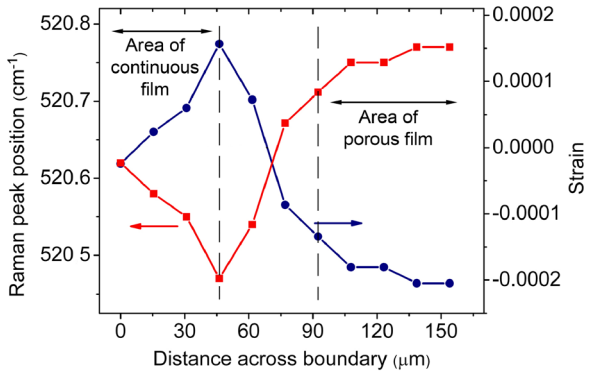

FIG. 6. Raman shift of the Si-Si vibration band (related to the substrate) on the left scale and corresponding strain on the right scale as a function of the distance across the boundary between the continuous and porous films. The dotted lines separate the area of the data obtained for the continuous film, the intermediate area, and the porous film.

behind the island edge, is compressively strained.[30] Thus, for both continuous and porous films, the Si substrate areas are probably compressively strained when located under the SiGe film areas, as schematically illustrated in Fig. 7.

The appearance of a compressive stress after high-temperature annealing in the Si substrate, when being located under a SiGe film, is suggested to have the following origin. The Ge atom diffusion into the Si substrate predominantly occurs via interstitial lattice sites.[31,32] The Ge atom introduction in the interstitial sites of the Si substrate can produce a compressive stress among neighboring Si atoms. In this case, a substantially lower Ge content is required to ensure the lattice mismatch compensation than in case of the Ge atoms located at the lattice sites. This is consistent with the formation of rather sharp Si/SiGe interfaces, which indicates, in particular, that the interdiffusion predominantly occurs by means of Si diffusion from the substrate into the SiGe film, whereas an essentially smaller amount of Ge atoms penetrates the Si substrate.

V. PL PROPERTIES

The low temperature PL spectra measured on both continuous and porous film areas are shown in Fig. 8. A rather

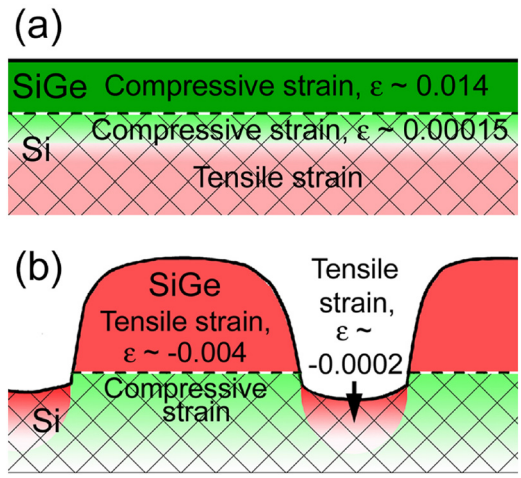

FIG. 7. Schematic illustration of the strain distribution in thin films with continuous (a) and porous (b) areas.

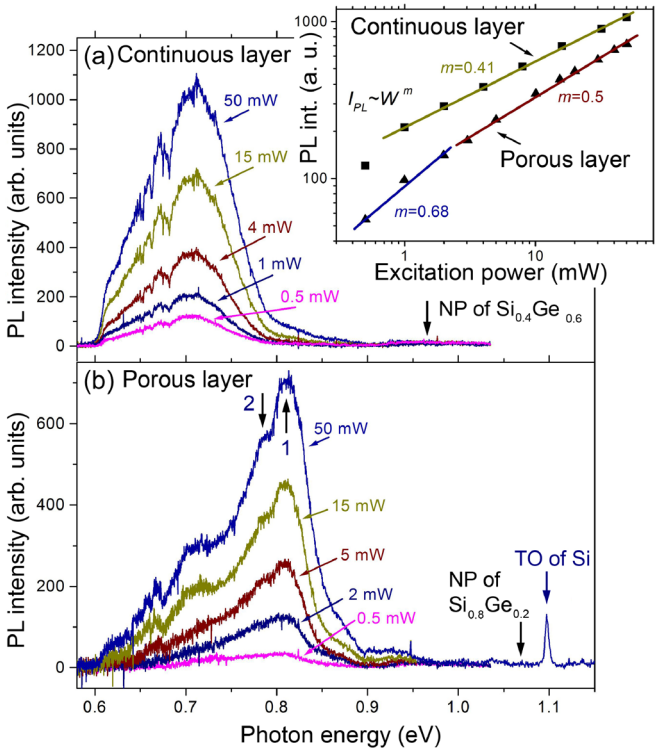

FIG. 8. Pump power dependences of the PL spectra of the continuous (a) and porous (b) film areas measured at about 10 K. The PL peak intensity as a function of the laser pump power for the continuous and porous film areas is shown in the inset. The arrows show the spectral position of the no-phonon peaks for SiGe with compositions $Si_{0.4}Ge_{0.6}$ and $Si_{0.8}Ge_{0.2}$ in (a) and (b), respectively. Arrows 1 and 2 in (b) show the positions of the D1 PL band (0.816 eV) of Si and of $Si_{0.8}Ge_{0.2}$ (0.775 eV), respectively, obtained according to our two Lorentzian line-shape fitting. The sensitivity limit of the infrared detector is about 0.6 eV.

broad PL band is observed ranging from about 0.6 eV to 0.9 eV in both cases. The absence of characteristic no-phonon (NP) and TO phonon peaks, which are typically observed for strained SiGe films,[33–35] indicates that the films are relaxed.[35,36] This is in agreement with the Raman data that showed the existence of only a weak strain in both films [Fig. 5(b)]. Therefore, the observed PL may be associated with deep energy levels created by the crystal defects, such as threading dislocations, which usually produce the so-called D bands in Si.[37,38] The spectral position of the D bands in the PL spectra depends on the preparation conditions of the SiGe films and their composition.[33,34]

The continuous SiGe film exhibits a broad PL peak centered at 0.7 eV [Fig. 8(a)]. This peak is distant from ~0.973 eV, which could be expected for the no-phonon PL peak position in the films with the nominal $Si_{0.4}Ge_{0.6}$ composition.[39] The PL spectra shown in Fig. 8(a) are similar to those of dislocated Si containing only the D1 line.[37,38,40,41] The similarity suggests that the observed PL peak also corresponds to the D1 line originating from the SiGe layer.

The PL peak of the porous film area is significantly blue-shifted with respect to the PL peak of the continuous film area, and it reaches a maximum at ~0.8 eV [Fig. 8(b)]. The difference of ~0.1 eV in the PL peak positions is about the same as the difference in the bandgaps between $Si_{0.4}Ge_{0.6}$ and $Si_{0.8}Ge_{0.2}$ alloys. The complex PL peak shape of the porous film area suggests that it can be deconvoluted in two peaks. The two Lorentzian line-shape fitting gave their location at 0.775 and 0.816 eV. The last value corresponds to the energy of the dislocation-related D1 band of crystalline Si,[37,38] and, therefore, it can be attributed to the dislocations in the Si substrate, which may propagate from the $Si/Si_{0.8}Ge_{0.2}$ interface down to the Si substrate. The PL peak at 0.775 eV can originate from the dislocation-related D1 band of the porous film, since its position in SiGe layers depends on the preparation conditions.[33,34] It is worth mentioning that the PL intensity of the porous film area is about two times smaller than that of the continuous film area. This can be the result of a more intense excited carrier recombination on the surface due to a larger area of porous film surfaces.[35]

Since the PL intensity from the SiGe layers is rather weak, the pump power PL dependences were obtained for the relatively strong pump-power densities (see inset of Fig. 8). At such excitation conditions, the PL intensities (I_{PL}) demonstrate sublinear dependences on the excitation power. The PL intensity is determined by

$$I_{PL}(W) \propto np, \tag{5}$$

where W is the pump power, n and p are the concentrations of the excited electrons and holes. The observed weak PL intensity indicates that the carrier concentration is governed by the rate $R(n,p)$ of nonradiative recombination by means of Auger processes which involve three charge carriers[42,43]

$$R(n,p) \approx C_1 n^2 p + C_2 np^2, \tag{6}$$

where C_1 and C_2 are the rate constants of the Auger processes. Since $R(n,p) \propto W$, and assuming that n and p have the same dependence on W, from Eq. (6) we obtain n, $p \propto W^{1/3}$, and, hence, $I_{PL}(W) \propto W^{2/3}$ according to relation (5). In the range of high excitation conditions, the multiphoton absorption becomes essential and leads to the excitation dependences weaker than n, $p \propto W^{1/3}$ and that was observed for charge carriers in Si.[44] This results in $I_{PL}(W)$ weaker than $I_{PL}(W) \propto W^{2/3}$, which is obtained here for the high excitation conditions of the SiGe layers (Fig. 8).

The porous area formation leads to a decrease of the PL intensity and to an increase in the power exponent m of the PL intensity dependence on the pump power (see inset of Fig. 8). These changes can be associated with an increase in the surface recombination rate, which causes a decrease in the free carrier concentration. Consequently, the PL intensity decreases, as observed in Fig. 8(b), and the exponent m of the PL intensity dependence on the pump power increases. The PL intensity of the continuous and porous films was measured as a function of the sample temperature for the constant excitation power of 30 mW. The obtained temperature behavior (not shown here) was similar to that of the dislocation-related PL from Si caused by thermal quenching.[45,46] The PL from the SiGe films almost quenches for temperatures higher than 150 K.

Dislocated Si exhibits several dislocation-related PL peaks, (D1-D2, in particular) if the crystal defects are introduced in Si using mechanical treatment[37,38] or electron,[47,48]

as well as ion[49] beam irradiations. However, if the dislocations appear as a result of thermal treatment of Si/Ge structures, this leads to the predominant formation of only one PL peak at about 0.8 eV.[40,41] This peak is associated with the D1 dislocation-related band in Si. The PL results obtained here for the porous SiGe film area also show the formation of the dislocation-related D1 band, which appears in the Si substrate, as well as in the $Si_{0.8}Ge_{0.2}$ porous film area. The fact that only one dislocation-related peak dominates in the PL spectra of SiGe layers, initiated by high-temperature annealing, is likely to be a common feature of the Si/Ge heterostructures. This suggests that the corresponding deep energy levels in Si and SiGe can be the result of the presence of Ge atoms in the interstitial lattice sites near the threading dislocations. This is in agreement with a compressive stress in the Si substrate, which may be due to the Ge atoms located in the interstitial lattice sites in Si.

VI. CONCLUSION

We have shown that the annealing of SiGe films at 850 °C leads to a gradual displacement of the boundary between continuous and porous film areas. The width of the boundary is about 100 μm. Both EDX and Raman spectroscopy data showed that the boundary displacement is accompanied by a decrease in the Ge content from about 60% to 20% when moving from the continuous to the porous film area. This is further accompanied by a change in the stress from a compressive in the continuous film area to a tensile in the porous film area. For the Si substrate, instead of the tensile stress, which should be expected due to the Si-Ge lattice mismatch, the annealing at 850 °C results in the appearance of a compressive stress. It is suggested that this occurs due to the Ge atom occupancy of the interstitial lattice sites in the Si substrate. The PL with the photon energies ~0.3 eV smaller than the SiGe bandgap is observed for both continuous and porous film areas. This PL can be associated with deep energy levels in SiGe caused by the crystal defects, such as threading dislocations. The PL spectra indicate that the presence of Ge in Si, as well as in SiGe, after annealing produces preferably only one type of radiative recombination centers, such as the D1 dislocation-related PL band. In agreement with the previous suggestion, these centers can be associated with the Ge atoms located at interstitial lattice sites near dislocation cores.

ACKNOWLEDGMENTS

The financial support from RSF Grant 14-22-00143 is gratefully acknowledged. The experiments were partly carried out using the equipment of and supported by CKP "NANOSTRUKTURY."

[1]C. M. Müller and R. Spolenak, Acta Mater. **58**, 6035–6045 (2010).
[2]A. Kosinova, O. Kovalenko, L. Klinger, and E. Rabkin, Acta Mater. **83**, 91–101 (2015).
[3]P. Jacquet, R. Podor, J. Ravaux, J. Teisseire, I. Gozhyk, J. Jupille, and R. Lazzari, Scr. Mater. **115**, 128–132 (2016).
[4]A. Shklyaev, L. Bolotov, V. Poborchii, and T. Tada, J. Appl. Phys. **117**, 205303 (2015).
[5]A. A. Shklyaev and A. V. Latyshev, Nanoscale Res. Lett. **11**, 366 (2016).
[6]A. A. Shklyaev and A. E. Budazhapova, Thin Solid Films **642**, 345–351 (2017).
[7]W. P. Huang, H. H. Cheng, G. Sun, R. F. Lou, J. H. Yeh, and T. M. Shen, Appl. Phys. Lett. **91**, 142102 (2007).
[8]D. Qi, H. Liu, S. Chen, C. Li, and H. Lai, J. Cryst. Growth **375**, 115–118 (2013).
[9]A. A. Shklyaev and K. E. Ponomarev, J. Cryst. Growth **413**, 94–99 (2015).
[10]Y. F. Lu, L. Zhang, W. D. Song, Y. W. Zheng, and B. S. Luk'yanchuk, JETP Lett. **72**, 457–459 (2000).
[11]A. B. Evlyukhin, C. Reinhardt, A. Seidel, B. S. Luk'yanchuk, and B. N. Chichkov, Phys. Rev. B **82**, 045404 (2010).
[12]V. Poborchii, A. Shklyaev, L. Bolotov, N. Uchida, T. Tada, and Z. N. Utegulov, Appl. Phys. Express **10**, 125501 (2017).
[13]A. I. Kuznetsov, A. E. Miroshnichenko, M. L. Brongersma, Y. S. Kivshar, and B. Luk'yanchuk, Science **354**, aag2472 (2016).
[14]M. Trautmann, F. Cheynis, F. Leroy, S. Curiotto, O. Pierre-Louis, and P. Muller, Appl. Phys. Lett. **110**, 263105 (2017).
[15]W.-K. Lee, S. Yu, C. J. Engel, T. Reese, D. Rhee, W. Chen, and T. W. Odom, Proc. Natl. Acad. Sci. U.S.A. **114**, 8734–8739 (2017).
[16]A. A. Shklyaev and A. E. Budazhapova, Appl. Surf. Sci. **360**, 1023–1029 (2016).
[17]G. K. Krivyakin, V. A. Volodin, S. A. Kochubei, G. N. Kamaev, A. Purkrt, Z. Remes, R. Fajgar, T. H. Stuchliková, and J. Stuchlik, Semiconductors **50**, 935–940 (2016).
[18]V. A. Volodin, M. P. Gambaryan, A. G. Cherkov, M. Stoffel, H. Rinnert, and M. Vergnat, Mater. Res. Express **3**, 085019 (2016).
[19]M. I. Alonso and K. Winer, Phys. Rev. B **39**, 10056–10062 (1989).
[20]V. A. Gaisler, V. A. Markov, M. P. Sinyukov, and A. B. Talochkin, Solid State Phys. **31**(8), 284–287 (1989).
[21]F. Pezzoli, L. Martinelli, E. Grilli, M. Guzzi, S. Sanguinetti, M. Bollani, H. D. Chrastina, G. Isella, H. von Känel, E. Wintersberger, J. Stangl, and G. Bauer, Mater. Sci. Eng. B **124–125**, 127–131 (2005).
[22]V. A. Volodin, D. V. Marin, V. A. Sachkov, E. B. Gorokhov, H. Rinnert, and M. Vergnat, J. Exp. Theor. Phys. **118**, 65–71 (2014).
[23]T. S. Perova, J. Wasyluk, K. Lyutovich, E. Kasper, M. Oehme, K. Rode, and A. Waldron, J. Appl. Phys. **109**, 033502 (2011).
[24]V. A. Volodin, M. D. Efremov, A. S. Deryabin, and L. V. Sokolov, Semiconductors **40**, 1314–1320 (2006).
[25]H. Chen, Y. K. Li, C. S. Peng, H. F. Liu, Y. L. Liu, Q. Huang, and J. M. Zhou, Phys. Rev. B **65**, 233303 (2002).
[26]Y. Ishikawa, K. Wada, D. D. Cannon, J. Liu, H.-C. Luan, and L. C. Kimerling, Appl. Phys. Lett. **82**, 2044–2046 (2003).
[27]C. Zhao, S. Wen, Q. Hou, W. Qiu, Y. Xing, S. Su, and B. Cheng, J. Phys. Chem. Solids **90**, 87–92 (2016).
[28]E. Anastassakis, A. Pinczuk, E. Burstein, F. H. Pollak, and M. Cardona, Solid State Commun. **88**, 1053–1058 (1993).
[29]V. Poborchii, T. Tada, and T. Kanayama, Appl. Phys. Lett. **97**, 041915 (2010).
[30]R. Gatti, A. Marzegalli, V. A. Zinovyev, F. Montalenti, and L. Miglio, Phys. Rev. B **78**, 184104 (2008).
[31]D. Caliste, P. Pochet, T. Deutsch, and F. Lançon, Phys. Rev. B **75**, 125203 (2007).
[32]P. Pochet and D. Caliste, Mater. Sci. Semicond. Proc. **15**, 675–690 (2012).
[33]V. Higgs, E. C. Lightowlers, E. A. Fitzgerald, Y. H. Xie, and P. J. Silverman, J. Appl. Phys. **73**, 1952 (1993).
[34]K. Shum, P. M. Mooney, and J. O. Chu, Appl. Phys. Lett. **71**, 1074–1076 (1997).
[35]R. L. Peterson, H. Yin, and J. C. Sturm, MRS Online Proc. Libr. Arch. **809**, B8.4.1–B.8.4.6 (2004).
[36]K. N. Galkin, R. I. Batalov, R. M. Bayazitov, H. A. Novikov, V. A. Shustov, D. A. Bizyaev, P. I. Gaiduk, G. D. Ivlev, and S. L. Prokopyev, Phys. Status Solidi C **10**, 1824–1827 (2013).
[37]N. A. Drozdov, A. A. Patrin, and V. D. Tkachev, JETP Lett. **23**, 597–599 (1976).
[38]R. Sauer, J. Weber, J. Stolz, E. R. Weber, K. H. Küsters, and H. Alexander, Appl. Phys. A **36**, 1–13 (1985).
[39]J. Weber and M. I. Alonso, Phys. Rev. B **40**, 5683–5693 (1989).
[40]A. A. Shklyaev, S. P. Cho, Y. Nakamura, N. Tanaka, and M. Ichikawa, J. Phys.: Condens. Matter **19**, 136004 (2007).
[41]C. D. Poweleit, C. W. Hu, I. S. T. Tsong, J. Tolle, and J. Kouvetakis, J. Appl. Phys. **101**, 114312 (2007).
[42]V. N. Abakumov, V. I. Perel, and I. N. Yassievich, *Nonradiative Recombination in Semiconductors* (PNPI RAN, St. Petersburg, 1997/ North-Holland Publishing, Amsterdam, 1991).

[43]M. Fukuda, *Optical Semiconductor Devices* (Wiley, New York, 1999).
[44]A. A. Shklyaev, A. V. Latyshev, and M. Ichikawa, Semiconductors **44**, 432–437 (2010).
[45]H. Lee and S. H. Choi, J. Appl. Phys. **85**, 1771–1774 (1999).
[46]A. A. Shklyaev, Y. Nakamura, F. N. Dultsev, and M. Ichikawa, J. Appl. Phys. **105**, 063513 (2009).
[47]L. Fedina, A. Gutakovskii, A. Aseev, J. V. Landuyt, and J. Vanhellemont, Philos. Mag. A **77**, 423–435 (1998).
[48]L. Xiang, D. Li, L. Jin, S. Wang, and D. Yang, J. Appl. Phys. **113**, 033518 (2013).
[49]N. A. Sobolev, A. E. Kalyadin, V. I. Sakharov, I. T. Serenkov, E. I. Shek, K. V. Karabeshkin, P. A. Karasev, and A. I. Titov, Tech. Phys. Lett. **43**, 50–52 (2017).

View publication stats